

Article

Separation Process and Microstructure-Chemical Composition Relationship of Cenospheres from Lignite Fly Ash Produced from Coal-Fired Power Plant in Thailand

Sorachon Yoriya *  and Phattarathicha Tepsri

National Metal and Materials Technology Center, 114 Thailand Science Park, Pahonyothin Road, Khlong Nueang, Khlong Luang, Pathum Thani 12120, Thailand; phattarathicha.tep@mtec.or.th

* Correspondence: sorachy@mtec.or.th

Received: 13 July 2020; Accepted: 3 August 2020; Published: 10 August 2020



Abstract: The cenosphere is one becoming a focus of the power plant in terms of value addition and ash management. This study presents a systematic investigation and characterization of physical properties, morphological structures, and chemical composition of cenospheres separated from fly ash produced from the Mae Moh coal-fired power plant, Thailand. To our knowledge, this is the first report on cenospheres separation from Mae Moh class C fly ash, with high calcium content ~24 wt.%, by adopting the traditional wet separation method (using water as the medium) to separate the lightweight cenospheres. Various effects of process parameters (fly ash-to-water ratio, stirring method, ultrasonication, and size classification) were designed to examine the cenosphere recovery yield in comparison. The result has revealed the limit of physical stirring-settling effect associated with the cenospheres content by nature governing the percent recovery. The bulk cenospheres were subject to size sieving into different sized fractions, with the structure-chemical composition relationship established for more insight. The particle diameter/shell thickness ratio revealed its significant correlation with the aluminosilicate glass composition, with the relating cenosphere shell structures (single-ring and porous) mapped to compare for a better elucidation of their structure-property relationship. The phase composition was also studied.

Keywords: cenospheres; fly ash; wet separation; chemical composition; aluminosilicate; SiO₂; Al₂O₃; power plant

1. Introduction

Fly ash is one of the byproduct produced from the coal-fired power plant through the combustion process for power generation. Mae Moh coal-fired power plant (Lampang province, Thailand), the biggest one in the country, producing a large amount of byproducts each year, including bottom ash, fly ash, and gypsum [1–4]. Mae Moh lignite fly ash having good pozzolanic and binding properties enabling it an excellent choice mainly for construction [3,5,6]. In Thailand, the most effective use of fly ash is in the area of concrete [6–10]. Fly ash is known to be used to substitute Portland cement Type 1 [11], which can reduce production costs while increase the product properties. Over decades, lignite fly ash has been used in many important construction industries, such as concrete pipe and pile manufacturing and in paving blocks [7,10]. The large-scaled construction projects include Khun Dan Prakarn Chon Dam in Nakhon Nayok, Rama 8 Bridge's abutment, MRT underground tunnels in Bangkok, footings of the Suvarnabhumi International Airport, and also construction abroad in the Xayaburi Dam and Nam Theun 1 Dam project in Laos [12]. Considering the volume of fly ash and its value as concrete, fly ash is a cement-substituting material used to improve concrete

properties, such as durability, improved workability, and long-term strength. The Thai lignite fly ash has high calcium; the high calcium content has pushed fly ash to the utilization limit in various mass applications [3,5,6]. According to the concept of the circular economy focusing on resource reuse and recycling, focusing maximizing the efficient use of existing resources, minimizing the waste—thus reducing the environmental impact—are principal concerns of the power plant.

A value-added material or a subproduct mixing with fly ash is cenospheres. Cenospheres are hollow, spherical shaped particles, mostly open-pore in nature, and a lightweight material. Cenospheres are of a similar chemical composition to fly ash as their mineral composition is dependent upon the geological and chemical features of coal source and the combustion conditions forming them [13–15]. Cenospheres have superior properties are lightweight, chemically inert and have good flowability, improved workability, good insulation, good thermal resistance, and excellent mechanical strength [16–18]. With their distinctive properties, they have become a highly in-demand material in many specialized applications, such as light weight additive or filler in construction, cement and concrete [19–22], polymer composites [23–25], fabricated composite in railway systems [26], sound-absorbing material [27], thermal insulation products [17,28–30], composite for metal matrices [31], and ceramic foam [32,33]. Cenospheres offers significant advantages in a wide range of industrial processes, including manufacturing, product improvement, and cost reduction purpose. Utilizing cenospheres in the products, performance relating to properties of material depends considerably on the cenospheres characteristics, which include physical properties, morphological structure, and chemical composition. A good understanding of cenosphere characteristic properties is considerably essential to not only the optimization of cenospheres recovery parameters, but also the development of effective strategies to recover cenospheres with a controllable quality.

The methods of cenosphere separation are wet separation and dry separation. For the wet separation in liquid medium, cenospheres can be generally separated from fly ash with the mechanism based on the density difference between particles and liquid. Wet separation is the method mostly used to separate lightweight or low-density cenospheres. The optimization of cenospheres recovery process to obtain high recovery yield (yet limited by their content by nature) and good quality of cenospheres, is important. Furthermore, a clear understanding of how the structural features corresponding to the composition of cenospheres as a result of the particle formation process is essentially needed [15,16,34]. Whereas the dry separation is the relatively complicated method that requires the more advanced technology to efficiently classify the ash particles, the mechanism involves pneumatic separation or air classification as the separation efficiency depends remarkably on physical characteristics such as the size, shape, and density of the ash particles [18,29,35,36].

Cenospheres are widely known as a lightweight material with a density less than 1.0 g/cm^3 , with their concentration by weight in fly ash as low as $< 2\%$ [14,37,38]. With wet separation, cenospheres float on the water surface and can be collected by decanting the floating layer. There have been many reports on investigation of cenospheres yield, morphological structure, chemical composition, and mineral phases of cenospheres collected from various power plants [16,17,34,37,39–45]. Those studies presented the cenospheres recovery, mostly from class F fly ash (in accordance with American Society for Testing and Materials (ASTM) C618) [46], and peculiar properties of ash cenospheres that strongly depend on the coal type used and the power plant conditions. The main focus of this work is to systematically investigate technical possibilities of obtaining cenospheres from the wet separation process, emphasizing the correlation study of structures and properties of the harvested cenospheres from the high-calcium class C fly ash produced from Thai power plant. The physical properties, morphological and microstructural characteristics of particles, and chemical composition have been examined. The results from this study are anticipated to be a starting base of data in the elucidation of Mae Moh cenospheres recovery yield and their properties, and the evaluation of potential utilizations of the coal combustion product.

2. Materials and Methods

Fly ash was collected from Unit 12 station of the lignite coal-fired power plant located in Lampang province, in the northern region of Thailand. Mae Moh power plant uses pulverized coal combustion in superheated boilers to generate electricity. The lignite coal used contains high calcium oxide and sulfur contents, thereby leading to severe slagging problems frequently to occur and reflecting high CaO and SO₃ in fly ash [4,5]. At Mae Moh power plant, flue-gas desulfurization (FGD) systems were installed for pollution control, as the FGDs absorb gaseous SO₂ from flue gas and produce gypsum byproduct. The general characteristic properties of fly ash sample are shown in Table 1.

Table 1. General characteristic properties of the fly ash sample.

Item	Unit 12
Density (g/cc)	2.48
%Free lime	1.43
%SO ₃	2.72
Average particle size ($D [4,3]$, μm)	41.51

Particle size distribution of the fresh fly ash sample were demonstrated in Table 2. Fineness of the fly ash sample was analyzed by wet sieving method by following the procedure in the ASTM C618 [46]; the amount of material retained on the 45- μm sieve (325 mesh) was determined.

Table 2. Particle size distribution (wt. %) of the fly ash sample.

Sample	Size Distribution (Wt.%)					
	<1 μm	1–10 μm	10–50 μm	50–100 μm	100–250 μm	250–500 μm
Fresh fly ash	8.13	32.66	33.08	14.33	10.89	0.91

2.1. Cenospheres Separation

The lignite fly ash sample was subject to wet separation. In this study, the sink-float method was employed to separate the lightweight cenospheres from the bulk fly ash, as the separation efficiency is based on the gravity settling. Water was used as the medium for both methods.

Different experimental sets were designed to investigate the maximum cenospheres recovery and the separation efficiency as dependent upon the process parameters. In this study, the effects of process parameters on the cenospheres yield were studied. For the sink-float method, the fly ash sample was added into water at different fly ash-water weight ratios (g/mL). Those varied parameters are fly ash content in water medium (1:5 (20 wt.%), 1:10 (10 wt.%), 1:20 (5 wt.%), 1:40 (2.5 wt.%), 1:80 (1.25 wt.%) fly ash-to-water ratios), stirring method (manually and ultrasonically), and size sieving for the starting fly ash prior to cenospheres separation. For the stirring procedure, mechanical stirring and ultrasonication (40 Hz) were employed. The mixtures were repeatedly stirred before leaving them to settle. It should be noted herein that a spontaneous imbibition is a measure of particle-level wettability. In this circumstance, water does not experience spontaneous imbibition into dry fly ash; however, wettability of the particles with intra-porous grains and accessible porosity is more pronounced for water to imbibe the ash particles [47]. Thus, in this study mixing procedure was adopted to facilitate such imbibition process for preparing the suspension prior to sedimentation and separation, while the fly ash sample was presumed to have a certain amount of such accessible porosity [18]. The effect of size classification for the starting fly ash before mixing with water was studied. For each experimental batch, the fresh fly ash was screened by wire mesh sieves into four different sizes: <45, 45–105, 106–250, and >250 μm . Then these fractions were subject to cenospheres wet separation to particularly determine the cenospheres content in each size fraction. The cenospheres recovery yield was determined by the weight of cenospheres collected from each batch of size fractions with respect to the sum of cenospheres,

which was normalized to 100% (see the plots in Figure 1e). The purpose of this experiment is to compare the cenospheres yield with that obtained from the non-sieving condition. The mixtures were stirred to ensure the well mixing between fly ash and water. After stirring, the suspensions were allowed to settle for different time and pH was measured. The separation process was carried out at ambient temperature.

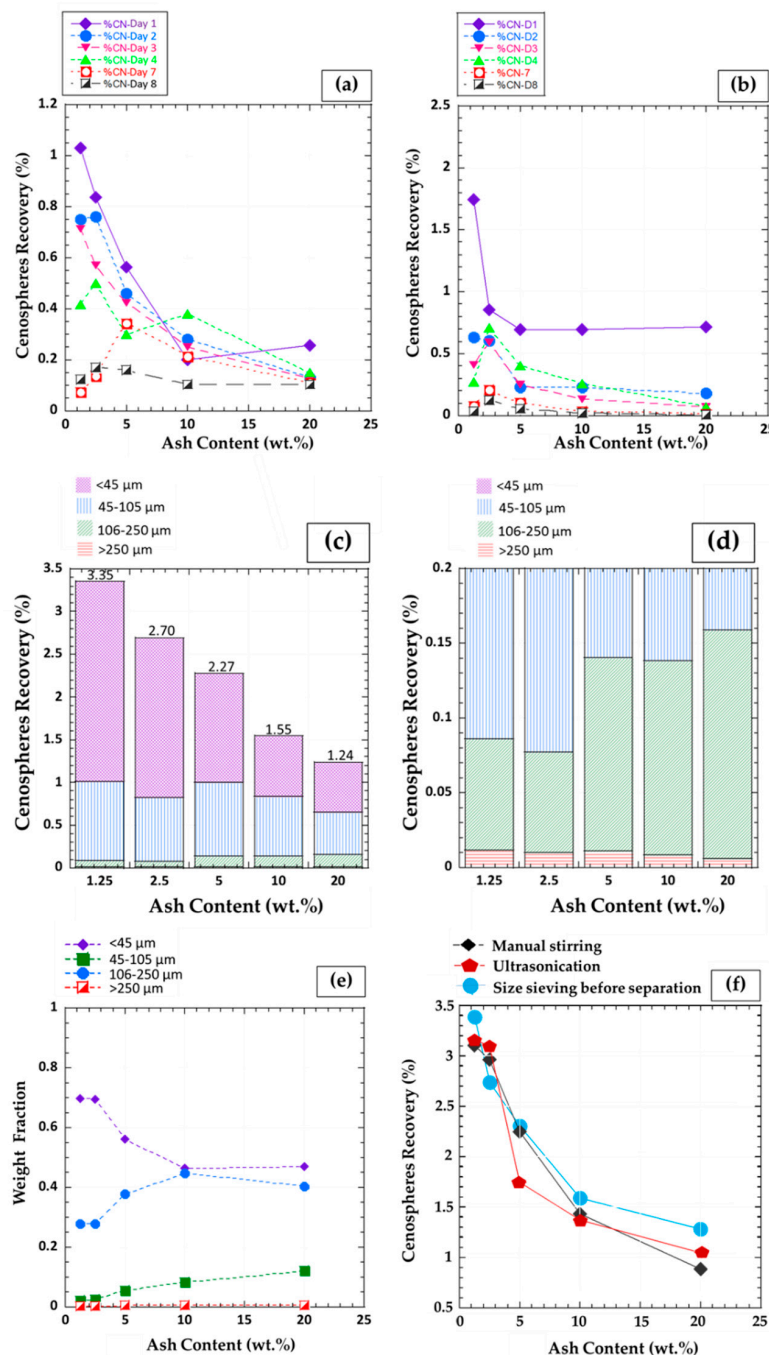


Figure 1. Plots of percentage recovery of cenospheres collected by sink-float method, using different ash contents, an eight-day period. The mixtures were (a) manually stirred for 10 min; (b) ultrasonicated for 30 min. (c,d) The percent cenospheres recovery obtained from using the starting fly ash being sieved into four sized fractions (<45, 45–105, 106–250, >250 μm) prior to the cenospheres separation; (d) is the zoomed-in plot for the conditions of 106–250 and >250 μm. (e) Plots of weight fraction of the data shown in (c,d) against ash content. (f) Overlay plots of accumulative percent cenospheres recovery against ash content for the data shown in (a–d).

After separation, cenospheres were harvested from the surface of liquid. The floating part, the cenospheres layer, was collected by gently decanting, then filtered prior to oven drying at 105 °C for 48 h. The cenospheres were collected at different periods of time designed per experiment. The amount of the floating layer, namely the low-density cenospheres, collected from the water surface was taken to calculate the cenospheres yield as follows. The percentage of cenospheres recovery (%) = (weight of floating particles/weight of total fly ash) × 100. The accumulative yields (in Figure 1) were calculated in terms of the total quantity of the collected floating particles as using various separation conditions, and their sum was normalized to 100%.

After drying process, the bulk cenospheres obtained from the one-day collection condition were sieved into a series of four size fractions (<45, 45–105, 106–250, and >250 µm) for further characterization. Density, particle size, and weight fraction of the sieved fraction were examined and compared as a function of size range and morphology.

2.2. Fly Ash and Cenospheres Identification

Physical properties, morphologies, and chemical composition of fly ash and the collected cenospheres were investigated. Apparent density was determined by ultracycrometer (Ultracycrometer 1200e, Quantachrome Instruments, FL, USA). Helium gas is the preferred displacement fluid due to its small dimensions and ideal gas behavior for volume measurement of porous solids and powders [48]. The gas flow purge was set at 1.0 min and five runs were performed, with the set deviation of 0.0050%. Particle size and distribution of the fly ash sample and the collected cenospheres were characterized by laser particle size analyzer with dry dispersion units (Masterizer 2000, Malvern Instrument, Malvern, UK). The measurements were run in air dispersion medium, with air pressure of 2 bar. The average particle size by means of the volume mean diameter is shown in *D* [4,3]. Morphologies of fly ash and cenospheres, wall thickness and hollow structured were studied by scanning electron microscopy (SEM) (Phenom ProX, Eindhoven, Netherlands). The SEM imaging was performed under the accelerating voltage of 15 kV on the samples with no coating. The wall thickness was measured through a random cross-section analysis using SEM technique; three to five measurements were conducted on each cross-sectional view of wall thickness as the pictures were taken from the broken cenospheres shell. The results derived in this study were generally in the form of an average wall thickness of bulk cenosphere sample. ImageJ was employed for the analysis of particle size and wall thickness. The elemental analysis of each ash and cenosphere particle, and the small particles depositing on the cenospheres surface were determined by the SEM equipped with energy-dispersive spectroscopy (EDX); spot analysis was carried out for the specific areas of interest on the particles. The EDX analysis results in terms of the compositional data are expressed in weight-percent (wt.%). Bulk chemical composition of fly ash and cenospheres were characterized by energy dispersive X-ray fluorescence (EDXRF; EDAX Smart Insight, ORBIS PC, NJ, USA). The detection limit for each element is 10 ppm, with intensity error set at 5%. The XRF results were presented in weight percentage of oxides. Concerning the aspect of statistics governing the properties of distribution, the mean and the standard deviation for the characterized results were considered to determine in this study. Powder X-ray diffraction patterns were recorded for the starting fly ash and the bulk cenospheres by a Bruker D8 ADVANCE diffractometer (Bruker, Bremen, Germany) (Cu K α radiation (1.540 Å), scan range $2\theta = 10\text{--}80^\circ$, scan step 0.5 s), with high speed data collection with LYNXEYE XE-T detector (Bruker, Germany). Phase analysis and peak interpretation were performed by DIFFRAC.EVA V5.1 software, database PDF2-Release2018.

3. Results and Discussion

3.1. Cenospheres Recovery Yield

The cenospheres yields obtained from different separation conditions are demonstrated in Figure 1a–e. The effect of mixing methods was particularly investigated by comparing between manual

stirring and using ultrasonication. Figure 1a,b shows the cenospheres yield obtained from different collection days (from Day 1 to Day 8) at various fixed fly ash-water ratios for the respective conditions of manual stirring and ultrasonication.

For a given collection time, the cenospheres yield tended to increase with decreasing the fly ash content in water; that is, the scheme under low fly ash/water ratios (1:20, 1:40, and 1:80), which correlated with the relatively lower concentration of fly ash (5, 2.5, and 1.25 wt.%, respectively) in the mixtures, is prone to result in a higher recovery yield of cenospheres. The dependence of cenospheres recovery yield on the factor of fly ash/water ratio was more pronounced when incorporating low fly ash, from 1.25 wt.%–5 wt.%, in water medium. This could be clearly observed particularly for the collection time within four days. Decreasing fly ash content to 1.25 wt.% in the mixture led to a high recovery percentage about 4–5 times more than that of the 10–20 wt.% contents. The maximum percent cenosphere recovery achieved was approximately 1 wt.% at Day 1 collection as using the most diluted 1.25 wt.% fly ash content condition.

For varying collection time, the plots of cenospheres yield against fly ash content appeared to be similar, especially for Day 1 to Day 4. On further increase in the collection time, the cenospheres yield tended to decrease in comparison. In this study, the mixtures were repeatedly stirred before leaving them to settle and the floaters were collected at each time. The recovery of the floaters was improved by a repeated stirring procedure [44]. While the longer collection period resulted in the relatively lower amount of cenospheres to be obtained. The graphs shown in Figure 1a,b comparing the conditions with and without ultrasonication are approximately in the similar pattern.

The effect of size classification for the starting fly ash on the cenospheres recovery yield is shown in Figure 1c,d; the weight fraction in Figure 1e is schematically demonstrated as an alternative view. It can be seen that the cenospheres collected from the small sized fractions (<45 and 45–105 μm) has higher yield than those collected from the relatively larger sized fractions (106–250 and >250 μm). This result has suggested that majority of Mae Moh cenospheres, > 80 wt.%, predominantly contained small particles, with a size of < 105 μm .

Figure 1f shows the accumulative plots of percent cenospheres recovery against the ash content. The accumulative cenosphere yields are in the range of ~0.8%–3.5%. These values were found in the similar ranges reported for various power stations [16,18,29]. The cenospheres recovered from fly ash contains predominantly cenospheres, porous char, individual ferrospheres, and ferrispheres [13]. These are the common characteristics of cenospheres, generally observed, and could to some extent contribute their weight fraction in the percent yield. The variation of cenosphere yield was believed to relate to the coal type, the coal mineralogy, and the combustion conditions [16].

From the overlay graphs (Figure 1f), it could be summarized that the separation efficiency is strongly dependent upon fly ash content. The cenospheres yield tended to increase for the more diluted concentrations, as the ascending curves seen when incorporating low ash concentrations. This is probably due to the effect of drag force (inter-particle interaction) governing the lateral segregation of light and heavy particles, thus enhancing the velocity of separation. The drag force leads to a formation of fingering flow structure along the gravitational direction in a sufficient solid concentration [18].

Both mechanical stirring and ultrasonication by applying sound energy to agitate particles in liquid revealed the similar result (Figure 1f), clearly indicating that the separation of cenospheres is independent on the physical mixing process. Similarly, size sieving aimed to deagglomerate particles prior to the sink-float separation did not show the improved cenospheres yield. One may assume that the cenospheres yield is limited by the stirring-settling effect associated with the cenospheres content by nature. In Figure 1e, the tendency of cenospheres yield for the large particle fractions is comparatively lower than that of the yield for the smaller particle fractions. This is attributed to the porosity and rough surface texture of the particle significantly influencing the movement and velocity of particles in the fluid [18,44].

However, it should be noted here that the fly ash-medium ratio of 1:10 is the optimal acquisition condition found widely used for cenospheres separation via the sink-float method [18,28]. A comparison

of the cenospheres yield obtained from different experiments is shown in Table 3. As the ash particles experienced the gravity separation, there could possibly be some broken cenospheres that become heavier and sink along with the small fly ash particles. Using water as a medium, it was possible to obtain cenospheres fraction composed of intact (undamaged) spheres by 2/3 of volume and a sediment part by 1/3 of volume consisting of small ash particles, cracked or fissured cenosphere ash particles, semi-coked particles, coked particles, slag fragments, and magnetic microspheres [18,37]. These were drawbacks of the gravity separation, that the cenosphere separation efficiency can be influenced by the fragments of various materials, broken spheres, and fine fly ash contaminated. Further, the fine fly ash particles could also form dense accumulation on the floating surface that in turn limits their sinking and eventually resulting in an increase in impurity of the cenosphere product, with such phenomenon possibly found for the separation of class C and class F fly ash [18]. The dense, fine fly ash particles found mixing with the collected cenospheres can be seen in this study (see the XRF imaging result). One may also be possible for the impurity inclusion is that the crushed but remaining unsinkable cenospheres could be found with the collected cenosphere fractions.

Table 3. Data comparing the recovery yield of cenospheres collected from different experimental conditions, particularly using fly ash-water ratio of 1:10 (10 wt. %).

Method	Condition	Cenospheres Recovery (%) ¹
Sink-float method	Manual stirring	1.43
	Ultrasonication	1.52
	Size sieving	1.55

¹ Five measurements were done and the SD of all data is less than 0.01.

3.2. Physical Properties of Cenospheres

As seen in Figure 2, the fresh fly ash exhibits reddish brown color. The fly ash sample used in this study contained mostly the small-sized particles; approximate weight fraction of ~74% for the particle size finer than 50 μm . Fineness of the fly ash sample was less than 34% of the material retained on the 45- μm sieve, which is the criterion for natural pozzolanic fly ash following the ASTM C618 [46]. Bulk density of the fly ash sample is 1.3 g/cm^3 , apparent density varied in the range of 2.4–2.9 g/cm^3 .

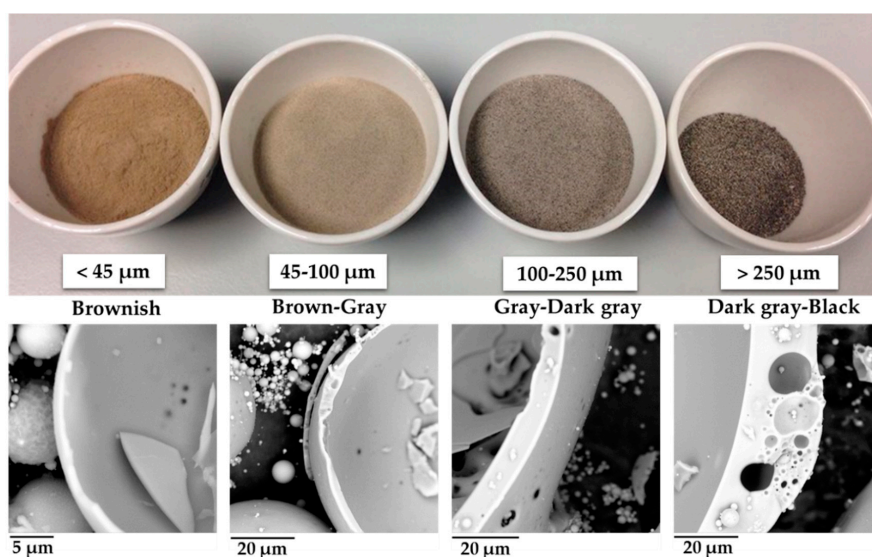


Figure 2. The bulk cenospheres were collected by sink-float method, using a fly ash-to-water ratio of 1:10. Shell thicknesses of those cenospheres in each size range were depicted.

The Mae Moh cenospheres separated from fly ash is sand-like texture, tiny granules. The collected cenospheres exhibits brownish grey color (Figure 2). Density of the bulk cenospheres obtained from different separation conditions are in the range between 0.95 to 1.03 g/cm³. These low densities indicate that the floating part collected is lightweight and cenospheric. The relatively high density could possibly be obtained for a prolonged soaking period. This is due to the larger amount of aggregates forming on the cenosphere surface in the form of calcium carbonate, hence determining the cenosphere recovery yield [28,49]. The calcium aggregates covering the surface of cenospheres can be seen in the morphological study of cenospheres.

The bulk cenospheres are typically of a broad size distribution, as seen in the literature [13,16,50,51]. The cenosphere samples after being sieved into four series of size (<45, 45–105, 106–250, >250 µm) have different colors varying from brownish to dark gray to black as the size increases (see Figure 2).

Density, average particle size of the cenospheres in each size fractions, and their weight fractions are shown in Table 4. The distribution of cenospheres is seen across various size fractions.

Table 4. Properties of cenospheres with various sizes.

Item	Size Range			
	<45 µm	45–100 µm	100–250 µm	>250 µm
Weight fraction (wt.%)	6.83	46.48	41.06	3.56
Density (g/cm ³)	1.40 ± 0.01	0.76 ± 0.01	1.24 ± 0.04	1.93 ± 0.01
Average size, <i>D</i> [4,3] (µm)	25.9	46.9	93.7	229.2

Note: The loss of particles is 2.07 wt.%.

Density of the starting bulk cenospheres before sieving is 1.03 g/cm³. After being classified in each size range, the density and the average particle size of the cenospheres were found to vary from 0.76 to 1.93 g/cm³ (see Table 4). For the size ranges between 45–100 and > 250 µm, it is apparent that the density increased with the particle size. While the density of the small fraction (<45 µm) sits outside this trend. The high density of this fraction (1.40 g/cm³) is attributed to the significant contribution of large amount of solid mass associated with the more densely packing of those small particles per a volume unit leading to such high density. The average particle size obtained in this study was found to vary from 25.9 to 229.2 µm (Table 4), as all the bulk cenospheres floated and formed a layer covering water surface. The particle size of predominantly silicate-based, hollow cenospheres lighter than water can vary from 5 up to 500 µm [37].

In Figure 2, the SEM images of the cenospheres shell thickness of different sizes are illustrated in comparison. It is clearly seen that the larger particle sizes tend to have a thick wall. The shell thickness of the cenospheres are in the range of ~0.7 to 21.6 µm, and the shell thickness was plotted as a function of particle diameter as demonstrated in Figure 3a. A large variation in shell thickness is seen with larger particle size. The plot has revealed that the shell thickness increased linearly with increasing the particle size, similar to those observed in the literature [14,16,50]. This clearly confirms that the increase in wall thickness strongly correlated with the increase in cenosphere particle size; the linear correlation coefficient is expressed in Figure 3a. The ratio of wall thickness to diameter was believed to strongly depend on the ash chemistry combustion condition, in terms of temperature-time history that the particles experienced in the furnace [16].

In relation to the particle diameter, the particle diameter/shell thickness ratio was also examined to elucidate the wall shell formation as a function of physical characteristics in terms of cenosphere particle. In Figure 3a, the particle diameter/shell thickness ratio for Mae Moh cenospheres obtained from lignite fly ash had a range from ~10 to 37. This ratio varied in a range of 19 to 38 for the smaller particles (average diameters 25.9 and 46.9 µm), and relatively constant at ~10 for the larger particles (average diameters 93.7 and 229.2 µm). A similar trend was observed for the cenospheres obtained from other fly ash sources; the particle diameter/shell thickness ratio was in the range from 20 to 30 for the smaller particles (diameters 50–140 µm), and remained constant at ~20 for the larger particles

(diameters 140–340 μm) [16,37]. It is interesting to note that the cenospheres of similar sizes may have a wide range of shell thickness, and the wall thickness broadly increases with increasing the particle diameter [16]. The shell thickness observed for the cenospheres from different sources is about 1–18 μm ; the ratio of wall thickness to particle diameter of cenospheres is generally limited to the range of <10.3% [14,16,18,50]. Agreeing well with those reported in the literature, the wall thickness-to-particle diameters of Mae Moh cenospheres were found in the ratio range of less than 10%; see Figure 4b.

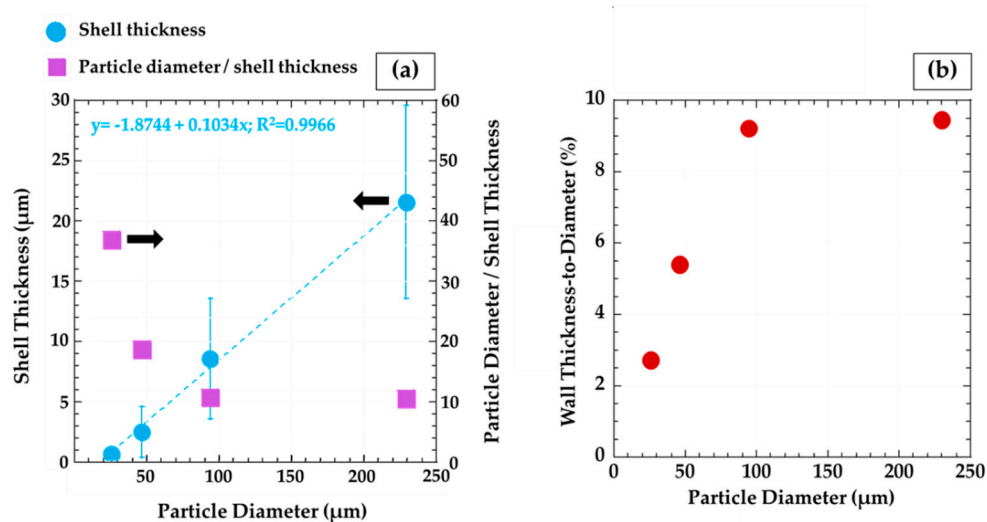


Figure 3. (a) Average shell thickness and particle diameter/shell thickness ratio plotted against particle diameter. (b) A plot showing a relation between percent wall thickness-to-diameter and particle diameter.

In Table 4, it can be seen that the majority (~87 wt.%) of the Mae Moh, lignite cenospheres have sizes between 45 and 250 μm . Whereas the relatively smaller fractions, ~7 wt.% and ~3 wt.% of total cenospheres, have sizes of intervals <45 and >250 μm , respectively. Comparatively reported by other studies, ~60%–94% of cenospheres collected from Class F fly ash have particle sizes between 45 and 250 μm , ~15% is possibly in the range of 150–200 μm , and ~5% is in the range of 200–250 μm [16,44]. The particle size distribution of cenospheres was found primarily to depend on the solid fuel preparation or crushing process before combustion, rather than the factors of coal composition and the coal combustion conditions [42].

3.3. Morphologies of Cenospheres

As seen in Figure 4a,b, the spherical particles were predominantly observed. Substantial differentiation of particle size is visible. Fly ash consists of spherical particles and some irregularities in size and shape. This is in good agreement with the result of particle size distribution varying broadly as shown in Table 2. The morphological structure of fly ash particles is controlled by the combustion temperature and the cooling rate of the boiler and its operating conditions [52]. During the combustion process, the heat causes the mineral matters to become fluid or volatile to react with oxygen. Whereas during the cooling process, the minerals may form crystalline solids, amorphous or condense spherical particles, or aggregates forming on the particle surface. In a boiler chamber of Mae Moh power plant, the organic materials in coal are combusted under high temperature and pressure, then the minerals transform into ash. The Mae Moh ash appeared to have crystal aggregates on the surface due to the slag occurrence in the boiler that is caused by quality of coal, mineral transformation and decomposition, and reaction chemistry of ash species due to heat [53].

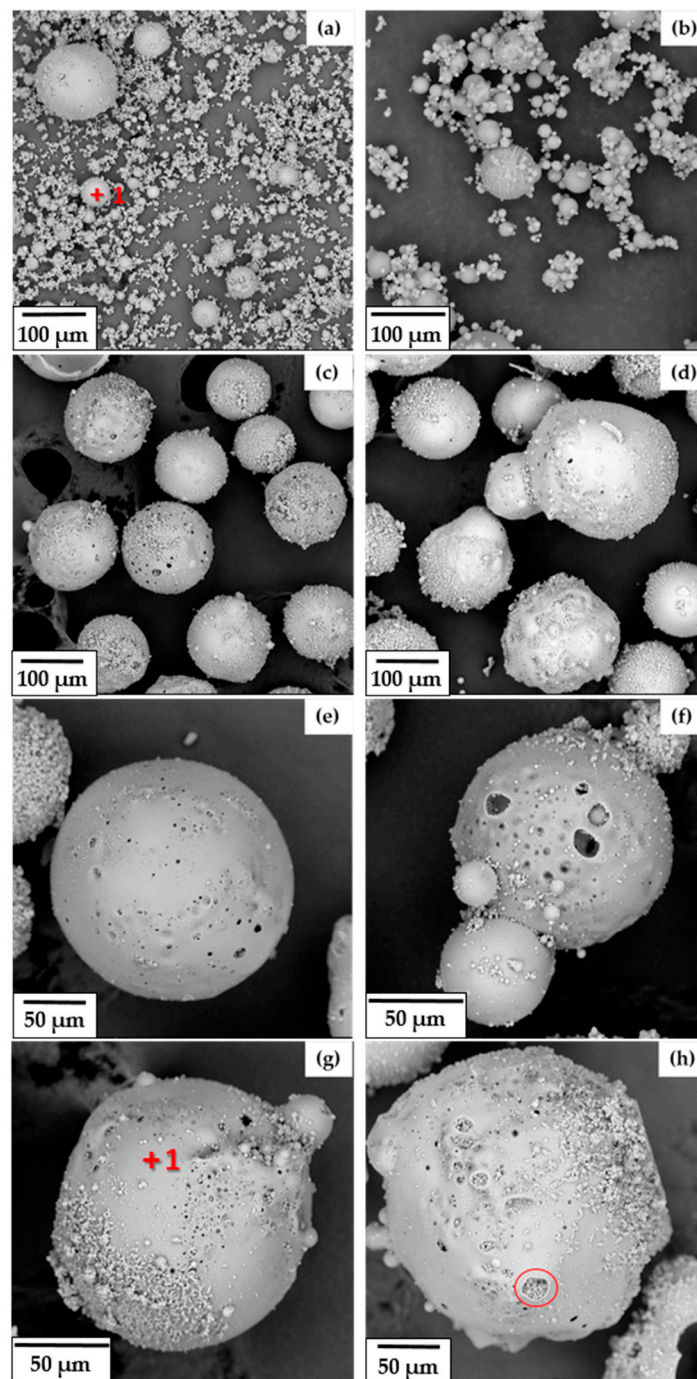


Figure 4. Scanning electron microscopy (SEM) images of (a,b) fly ash and (c–h) cenospheres collected by sink-float method, using a fly ash-to-water ratio of 1:10, a 2-h soaking period.

The SEM images of the collected cenospheres are shown in Figure 4c–h. The majority amount of cenospheres was found in the coarse grains. The size of cenospheres was obviously larger than fly ash. The smooth, dense, perforated, and vesicular spheres were commonly observed. Such dense and vesicular morphologies originate from fully and partly degasified melts of various minerals during burning [54]. Most of the obtained cenospheres contains the intact cenospheres, while damaged spheres or the partially broken spherical particles (Figure 5a, b) were periodically observed in a slight amount, which can be visible in the low magnifications. The crushed spheres could affect the cenospheres recovery yield and their quality, as mentioned earlier in the Section 3.1. For a specific

purpose concerning the porosity and surface area characteristics, such broken spheres could probably lead to higher surface area than the other intact cenospheres fractions; hence, an additional step, such as sieving, may be applied prior to utilization. In addition, it can be noticed that there are agglomerates and irregularly shaped particles appearing on the cenospheres surface, as clearly seen in Figure 4f–h. This could probably be due to the mineral (e.g., quartz) melting around the inter-particle contact and rapid cooling [52].

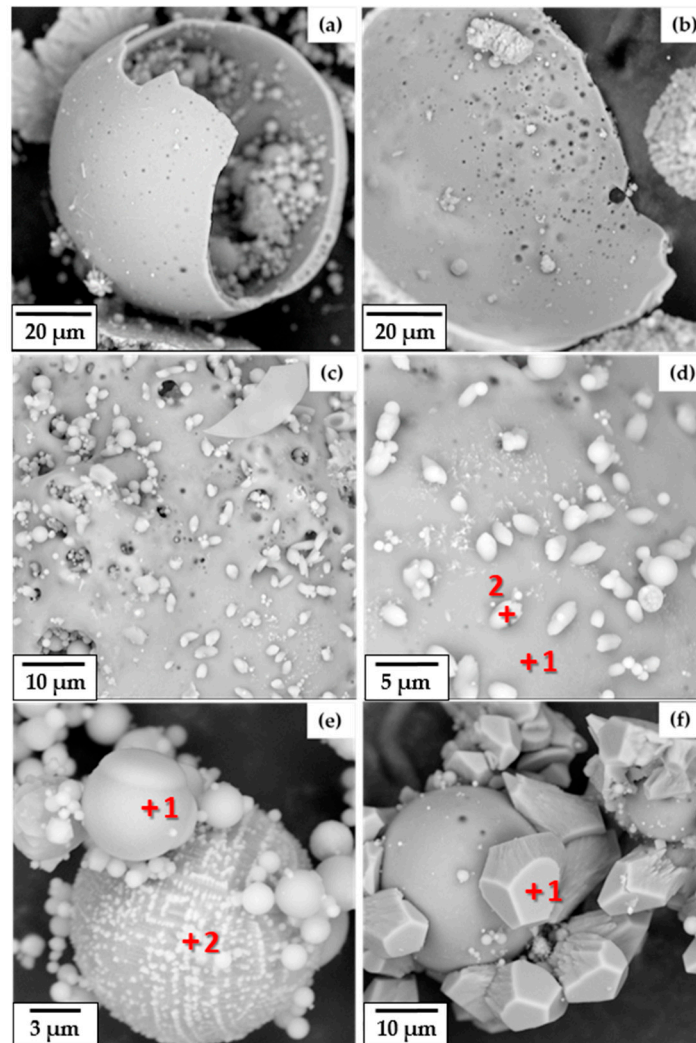


Figure 5. SEM images of cenospheres collected by sink-float method, using a fly ash-to-water ratio of 1:10: (a,b) broken particles of cenospheres, (c,d) small aggregates on cenosphere surface, (e) iron-rich particle, and (f) cenosphere particle covered by large aggregates.

The collected cenospheres are hollow spheres and have different structures: a single-ring structure, a porous shell structure (see the cross-sectional view in Figure 2). The single-ring structure was found for the small particles with the size $<100\ \mu\text{m}$, whereas the larger particles $>100\ \mu\text{m}$ the porous, thick shell structure was observed. The presence of cenospheres was due to the relatively higher viscosity of the melt forming an appropriate envelope possibly retaining the gas bubbles for a longer period while hardening [54]. Spheroids were rarely noticed containing in the collected cenospheres fractions, as clearly seen in Figure 4d. The surface texture of spheroids is porous and vesicular similar to those observed fly ash and the typical cenospheres. The spheroid structure was believed to originate from the spontaneous formation while fast cooling of cenospheres in a liquid or plastic state [54]. The quantity

of spheres and spheroids varies within the limit of 10–80% vol. in fly ash. In this study, plerospheres were also observed (see the circle in Figure 4h).

Cenospheres can be categorized into non-magnetic and magnetic particles. Depending upon physical characteristics, morphology, surface smoothness, shell thickness, and interior structure, the non-magnetic cenospheres can be transparent, and dark color. While the magnetic cenospheres are generally the particles with a spotty, porous, non-uniform shell, and dark spheres with white inclusions leading to opaque [18]. The high content of the spotty, non-uniform surface spheres is a result of the increase in Fe_2O_3 content in the range from 4 to 21 wt.% in the magnetic particle type with porous shells [14]. The iron oxide-rich phased particles were found in the magnetically separated fractions of Class F fly ash [55]. The white and grey is a result of carbonate and sulphate crystallization on the cenosphere surface. The yellow, orange to red, brown to black colors in cenospheres were found due to the occurrence of varying amount of iron and probably other trace colorants, such as Cr, Co, Cu, Mn within the glass network [13].

The iron sphere, Figure 5e, is the particle consisting of iron oxide mixed with amorphous aluminosilicate. This type of particle was found mixing with the collected cenosphere fraction. The SEM images present distinct diversity in morphologies, heterogeneous regions of iron oxides on the outer surface of the spheres. Through surface condensation or intermixing with the aluminosilicate, the iron oxide forms a variety of textures on the particle surface, interior of the particles, and even almost the entire particle covering with the iron oxide [52]. The iron ferrosphere structures of skeletal-dendritic, foamy porous globules, homogeneous blocklike, and platelike could be found on the surface of fly ash with magnetic properties and contain Fe_2O_3 content in a range of 20–88 wt.% [56].

Figure 5c,d,f is the pronounced effect of ash soaking period on the formation of calcite crystals on the cenosphere surface that leads to low quality of cenospheres to be obtained. Soaking the ash for a long period, the surface of the collected cenospheres was found covered with calcium carbonate crystallization consequently leading to different particle sizes obtained [13,28]. Figure 5f is the SEM image of cenosphere obtained from the eight-day soaking condition. Such a surface occurrence was described to be considerably due to a result of 'later' crystallization in the cenospheres separation process forming precipitates on the shell. Those precipitates, such as calcite, portlandite, dolomite and gypsum [13], are mainly a result of the dissolution of lime, periclase, and gypsum-anhydrite from the ash spheres during the wet separation, and after drying, they can transform into the more stable form by absorbing carbon dioxide from the air [18].

3.4. Chemical Composition

Analyzed by energy-dispersive spectroscopy (EDX), the cenospheres have an elemental composition similar to that of the starting fly ash. It was found that the elemental contents in the collected cenospheres include major and minor concentrations of Si, Al, Fe, Ca, S, Mg, Na, K, Ti, N. These elements were found on the fly ash and cenosphere particles from the spot analysis (Spot 1 in Figure 4a,g and Figure 5d,e). Analyzing the precipitates forming on the particle surface in Figure 5d, the EDX result of Spot 2 indicated that the precipitate mainly contained calcium concentration, 19.9 ± 1.30 wt.% Ca, comparatively larger than 2.2 ± 0.4 wt.% Ca of Spot 1 analyzed for the flat surface of cenosphere, whereas the larger size of precipitates forming aggregate crystals covering the cenosphere particle was found to contain even higher Ca content. The analyzed EDX result of Spot 1 in Figure 5f was 38.3 ± 1.10 wt.% Ca, 13.8 ± 1.50 wt.% C, and 47.9 ± 0.9 wt.% O. This composition is apparently in a close range to the theoretical molar mass percentage ratio of calcium carbonate, 40.04 wt.% Ca, 12.00 wt.% C, and 47.96 wt.% O [28,57,58]. For the iron sphere (Figure 5e), the enrichment of Fe content on the skeletal-dendritic structure (Spot 2) was much more pronounced, ~51–57 wt.%, compared to the Fe composition of the aluminosilicate surface of the ash particles, ~1–10 wt.%.

Upon the environmental aspect, it is noteworthy to mention that heavy metals and metalloids could present in fly ash, analyzed by its water solution. The pH values of water or aqueous solutions of fly ash are mostly neutral to highly alkaline with pH from 7–11, and the ions mainly containing in fly

ash solution are of Ca and S, and leachable trace elements possibly detected include As, Co, Cr, Mo, Ni, Se, Ti, V, and Zn [13,59–61]. The water solutions generated from Mae Moh fly ash in this study were found to be in high pH, at 12–13. Investigation of the heavy metals and trace elements in Mae Moh fly ash from lignite coal has been reported in the literature [2,3,62,63]. Mae Moh fly ash was found to contain a detectable concentration of many elements, including (ppm) Mn >> Ar, Zn > Cu, Cr, Ni, Pb, Mo, Co, Sb > Hg and >> Cd. These elements were leached out from fly ash under acidic conditions and various pH values. The variation of the trace elements is dependent on the combustion of different coals. Nonetheless, in fly ash from a single power plant, the concentration of the trace elements was found to vary on a daily basis of measurement [64]. The heavy metals and their fraction in fly ash are important concern for coal ash disposal and reuse options in commercial products. In addition to the heavy metals and trace elements, fly ash was also found to contain radioactive contamination, such as ^{235}U , ^{226}Ra , ^{238}U , ^{232}Th , and ^{40}K [65–67]. Acceptable radioactivity level is a key environmental factor for safe utilization of power plant wastes. Generally, most fly ashes have the radioactivity levels similar to that of natural materials. The high values in fly ash could be reduced to an acceptable limit in order to allow its utilization in mass construction.

The chemical composition of fly ash and cenospheres in the oxide forms was characterized by X-ray fluorescence (XRF) and shown in Table 5. The sum of SiO_2 , Al_2O_3 , and Fe_2O_3 in the fresh fly ash sample is 60.49%, which is in the range of 50%–70%, confirming its Class C fly ash according to ASTM C618 [46]. In general, cenospheres from different power plants have different bulk chemistry [14,16,18]. Nonetheless, SiO_2 and Al_2O_3 are found as the predominant oxide composition of cenospheres. The XRF has revealed that the composition of all cenosphere fractions are mainly aluminosiliceous (rich in Si and Al). All the cenospheres fractions are a multicomponent system with SiO_2 and Al_2O_3 contents in the intervals ~41–53 and ~19–25 wt.%, respectively. The fractions contained a relatively lesser Fe_2O_3 content of ~7–13 wt.%. Whereas CaO content is in the range of 6 to 16 wt.%. The stack columns are illustrated in Figure 6 for a better view of comparison. The compositions (SiO_2 , Al_2O_3 , Fe_2O_3 , and CaO) of the bulk cenospheres before being sieved seemed to be approximately in the average intervals of those compositions of cenospheres in each size range.

Table 5. Chemical composition of the collected cenospheres classified in different size ranges of < 45, 45–105, 106–250, >250 μm .

Item	Composition (Wt.%)							
	SiO_2	Al_2O_3	Fe_2O_3	CaO	SO_3	K_2O	TiO_2	MnO
Fly ash	32.12 ± 0.29	13.82 ± 0.19	14.55 ± 0.27	24.49 ± 0.05	12.03 ± 0.26	2.31 ± 0.02	0.55 ± 0.02	0.55 ± 0.01
Cenospheres								
Bulk	47.23 ± 0.56	22.92 ± 0.14	9.71 ± 0.48	10.89 ± 0.27	3.98 ± 0.12	4.54 ± 0.15	0.80 ± 0.02	0.06 ± 0.00
<45 μm	41.31 ± 0.16	19.61 ± 0.21	12.62 ± 0.15	15.50 ± 0.13	6.47 ± 0.10	3.76 ± 0.02	0.63 ± 0.00	0.11 ± 0.005
45–105 μm	53.39 ± 0.17	25.02 ± 0.06	7.84 ± 0.06	6.36 ± 0.11	1.88 ± 0.11	4.72 ± 0.07	0.78 ± 0.02	0.06 ± 0.001
106–250 μm	51.92 ± 0.23	23.72 ± 0.13	9.70 ± 0.11	8.28 ± 0.21	1.99 ± 0.04	3.57 ± 0.04	0.77 ± 0.005	0.06 ± 0.003
>250 μm	49.71 ± 0.93	20.80 ± 0.59	11.62 ± 0.99	11.56 ± 0.29	2.28 ± 0.31	3.23 ± 0.15	0.72 ± 0.02	0.08 ± 0.001

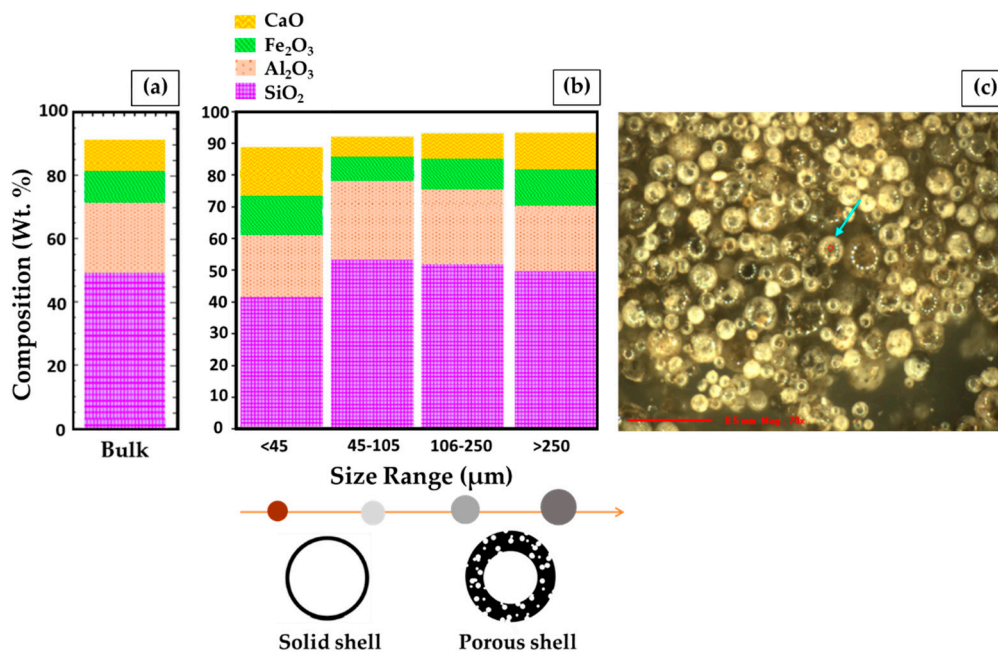


Figure 6. Oxide compositions of the cenospheres plotted in stack columns: (a) bulk cenospheres and (b) cenospheres after being sieved into different size fractions. The cenospheres were collected by sink-float method, using a fly ash-to-water ratio of 1:10. The data were taken from Table 5. (c) X-ray fluorescence (XRF) image of the collected cenospheres of size interval 106–250- μm , the arrow marked is the 150- μm size.

The physical characteristics in terms of color, size range, and shell structure of Mae Moh cenospheres are schematically presented to elucidate the formation structure of cenosphere shell in correlation with particle size and composition (see Figure 6a,b).

The brownish-to-light gray colored smaller particles (size intervals <45 and 45–105 μm) have a single-ring structure, whereas the grey-to-dark grey colored larger particles (size intervals 106–250 and >250 μm) have a porous shell. These are peculiar to the narrow fraction of cenospheres from Mae Moh fly ash. It was reported that the skeleton of cenospheres is encapsulated by ~90 wt.% of an amorphous glass phase, forming the structural stability of cenospheres over a wide range of temperature [13,50]. The cenospheres obtained from the XRF imaging (Figure 6c) are transparent, glassy, and opaque, with size distribution obviously seen even though the cenospheres were sieved into a narrow size fraction of 106–250 μm . This observation suggests that a narrow size fraction obtained from size sieving can yet remain a variation in particle size, from dense fine particles to large spheres. This is in agreement with the published report [16] that, for each narrow size fraction (e.g., 45–63, 63–75, 75–90, 90–106, 106–125, 125–150, 150–250, >250 μm), the relatively larger sized cenospheres were found to mix with the smaller sized cenospheres, and dense fly ash was clearly seen through microscopic investigation. The proportions of larger size increased substantially with an increase in cenosphere size fraction, as the larger size are of network structure.

Figure 7a, d show the pair dependence of SiO₂-Al₂O₃ and SiO₂/Al₂O₃-Al₂O₃ of the cenospheres in each size fraction. Figure 7a shows that the SiO₂ content in the cenospheres linearly depends on Al₂O₃ content. Comparing large particle group (45–105, 106–250, and >250 μm) to the small particle group (<45 μm), the SiO₂ content increased with the increased Al₂O₃ content. Among the large particle group, an opposite trend was observed; both SiO₂ and Al₂O₃ contents were found to slightly decrease with the increased particle size.

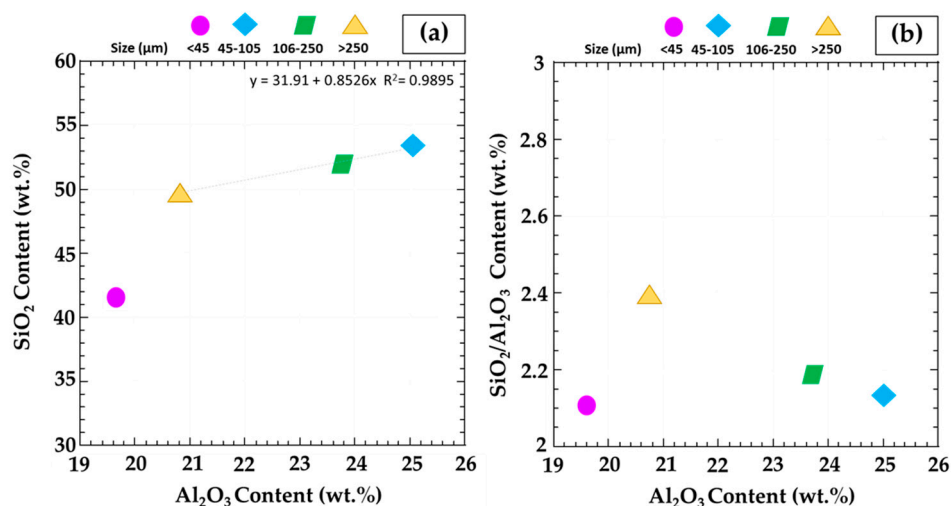


Figure 7. Dependence of (a) Al₂O₃ and SiO₂ contents and (b) Al₂O₃ content and SiO₂/Al₂O₃ ratio.

The SiO₂/Al₂O₃ ratio was plotted against Al₂O₃; see Figure 7b. The increased Al₂O₃ content seemed not to affect the SiO₂/Al₂O₃ ratio as the particle size increased. Correlating well with the data in Figure 7a, the SiO₂ content increased in a certain extent along with the increase in the particle size. As comparing with the starting fly ash, the SiO₂/Al₂O₃ ratios of cenospheres have lower values (2.11, 2.13, and 2.19 for the respective size fractions of <45, 45–105, and 106–250 μm) than fly ash (2.32). This observation is in a good agreement with those reported in the literature [13,28,68]. Except the size >250 μm, the value is slightly higher (2.39) than fly ash. Our previous study also found that, using acetone-water mixture as the separation medium, the SiO₂/Al₂O₃ ratios of the collected cenospheres were approximately in the close range (2.20–2.23) when using the fly ash/medium ratios from 1:2.5 to 1:10 [28]. This clearly confirms that cenospheres originated from the same pulverized coal combustion and the combustion process condition have the same major chemical composition.

Considering Figure 7b, the increase of SiO₂/Al₂O₃ ratio of the larger particles (▲) comparing to the smaller particles (◆, ■) is probably due to a phenomenon observed in many studies; the SiO₂ and Al₂O₃ contents reduced with increasing the particle size, while the extent of Al₂O₃ content reduction was measured in a very low amount with respect to the SiO₂ content [13,34,50]. The small particles (<45–250 μm, ●, ◆, ■) having lower SiO₂/Al₂O₃ ratio (~2.1–2.2) have a single-ring shell structure, whereas the larger cenospheres particles (>250 μm, ▲) having higher SiO₂/Al₂O₃ ratio (~2.3) have a porous wall shell structure, more likely in a network shell formed structure. An observation was reported on the relation between the SiO₂/Al₂O₃ ratio and the shell structure for the cenospheres separated from Class F fly ash. A high SiO₂/Al₂O₃ ratio (2.57) was found favorably to form small particles (<25 μm) with a spherical shape and the single-ring shell structure, while the relatively larger cenosphere particles (63–150 μm) with a network structure have a relatively lower SiO₂/Al₂O₃ ratio (1.64–1.8) [16]. To this point of view, it is interesting to note herein that there is a significant variation in chemical composition and cenospheres yield across the power stations and fly ash sources. The chemistry in cenospheres is strongly governed by the process of ash cenospheres formation in the furnace. The chemical composition of the molten droplets associated with the temperature in the furnace considerably determined the particle size of cenospheres [16,69]. The formation of large particle size was attributed to a result of an increased Al content that increases viscosity of the molten droplets, in turn stabilizing them during the expansion, rather than exploding into small fragments [18]. Besides, the higher SiO₂/Al₂O₃ ratio was suggested as an index parameter for a lower ash sintering temperature, favoring a ring structure [16,70].

Cenospheres from combustion of coal of various origins were found in different structures and compositions. Taking into account the physical-chemical parameters, cenosphere formation is affected by the chemical and phase composition of minerals inclusion of the initial coal and the combustion

operating conditions. A geochemical indicator of cenosphere composition is the $\text{SiO}_2/\text{Al}_2\text{O}_3$ ratio, characterizing the aluminosilicate minerals of coal from which cenospheres are formed. This reflects the morphological type of cenospheres with porous shell to mainly contain mullite crystals, which is the main crystalline phase as a result of the thermochemical conversion of aluminosilicate minerals through the activated amorphous state under high temperatures [50,51,68]. The phase-mineral composition of ash spheres includes not only various inorganic constituent phases of non-crystalline (amorphous) and crystalline (mineral) phases, but also organic matters (e.g., char and semi-coke) and fluid constituent such as liquid moisture and gas-liquid inclusions. The fundamentally important details were well described available in the literature [54,68].

3.5. Phase Composition

Figure 8a,b showed X-ray diffraction patterns for the fly ash sample and the bulk cenospheres, respectively. The XRD has resulted in the occurrence of both amorphous and crystalline phases, identifying fly ash and cenospheres a multicomponent system of minerals and phases. In Figure 8a, the phase composition found for Mae Moh fly ash sample includes anhydrite (CaSO_4), mullite ($3\text{Al}_2\text{O}_3 \cdot 2\text{SiO}_2$), quartz (SiO_2), Lime (CaO), magnetite (Fe_3O_4), potassium magnesium silicate ($\text{K}_2\text{MgSi}_5\text{O}_{12}$), portlandite ($\text{Ca}(\text{OH})_2$), merwinite ($\text{Ca}_3\text{Mg}(\text{SiO}_4)_2$), and srebrodolskite $\text{Ca}_2((\text{Fe}1.559\text{Al}0.441)\text{O}_5)$. Fly ash consists basically of aluminosilicate glass, minor mineral matter with high silicate abundance and dominant oxide tendency, and char; the major minerals and phases are mullite, quartz, char, kaolinite-metakaolinite, and hematite, while the minor minerals are cristobalite, plagioclase, K-feldspar, anhydrite, melilite, and corundum [49,68,71]. Height of the amorphous halo observed at $\sim 18^\circ$ – 38° (in Figure 8a) reflects the information for the non-crystalline or poorly crystallized phases. The inorganic amorphous matter was found due to the partial dehydroxylation and destruction of clay minerals, thus forming such poorly crystallized matter from the liberated organically bound elements during the coal combustion [68]. The phase composition of the bulk Mae Moh cenospheres was found to include calcite (CaCO_3), mullite, anhydrite, quartz, magnetite, and ettringite ($\text{Ca}_6\text{Al}_2(\text{SO}_4)_3(\text{OH})_{12} \cdot 26\text{H}_2\text{O}$) (see Figure 8b). The cenospheres are more abundant in mineral matter, including mullite and calcite, than the bulk fly ash [68]. The cenosphere shell consists of the majority of glass phase (70–90 wt.%), mullite, and quartz, whereas the minor minerals of cristobalite, potassium feldspar, plagioclase, hydromica, gypsum, and iron oxides were considered as impurities [16,37,51,54].

The phase analysis has revealed that mullite, anhydrite, and quartz identified in the fly ash sample and the bulk cenospheres were found to have the same lattice parameters. The lattice parameters of those phases are, respectively, as follows: $a = 7.5840 \text{ \AA}$, $b = 7.6930 \text{ \AA}$, and $c = 2.8900 \text{ \AA}$ (orthorhombic); $a = 6.9933 \text{ \AA}$, $b = 7.0017 \text{ \AA}$, and $c = 26.2411 \text{ \AA}$ (orthorhombic); and $a = 4.9650 \text{ \AA}$ and $c = 5.4240 \text{ \AA}$ (hexagonal). The obtained lattice parameters of mullite are in the range of known mullite compositions found in the concentration interval 57–92 mol% Al_2O_3 [72], particularly close to the composition of a mullite solid solution containing ~ 64 mol% Al_2O_3 in the nonmagnetic cenospheres with the crystallite size of $\sim 200 \text{ nm}$ [14]. The quartz component identified in the fly ash and cenospheres is the characteristic of the original coal, with such lattice parameters mentioned above indicating a peculiarities associated with the defect structure of quartz with aluminum ions probably embedded in the lattice due to dissolution of quartz in the molten glass phase during the cenosphere formation [14,42].

Besides, a noticeable difference observed is magnetite; the magnetite structure of the bulk cenospheres collected in this study is orthorhombic ($a = 5.9340 \text{ \AA}$, $b = 5.9250 \text{ \AA}$, and $c = 16.7520 \text{ \AA}$), whereas that of fly ash is cubic ($a = 8.3778 \text{ \AA}$). The formation of the ash cenospheres involves fundamentally the chemical oxidation reactions, the resulting gas generation, and particle expansion [69]. Within the Fe-S-O molten droplet precursor, the reactions consume sulfur dioxide gas while solidifying and forming the ash cenospheres. As such, the cenospheres contain sulfur in the shell and magnetite formed as the dominant final phase of iron oxide. Compared to the small ash particles, different stoichiometric ratios of elements constructing phases, herein magnetite, in the large cenosphere

shell could be possible in such a case of continuous oxidation reactions and varied temperatures associated with viscosity of the molten droplet precursor resulting in different reaction rates for the cenosphere formation.

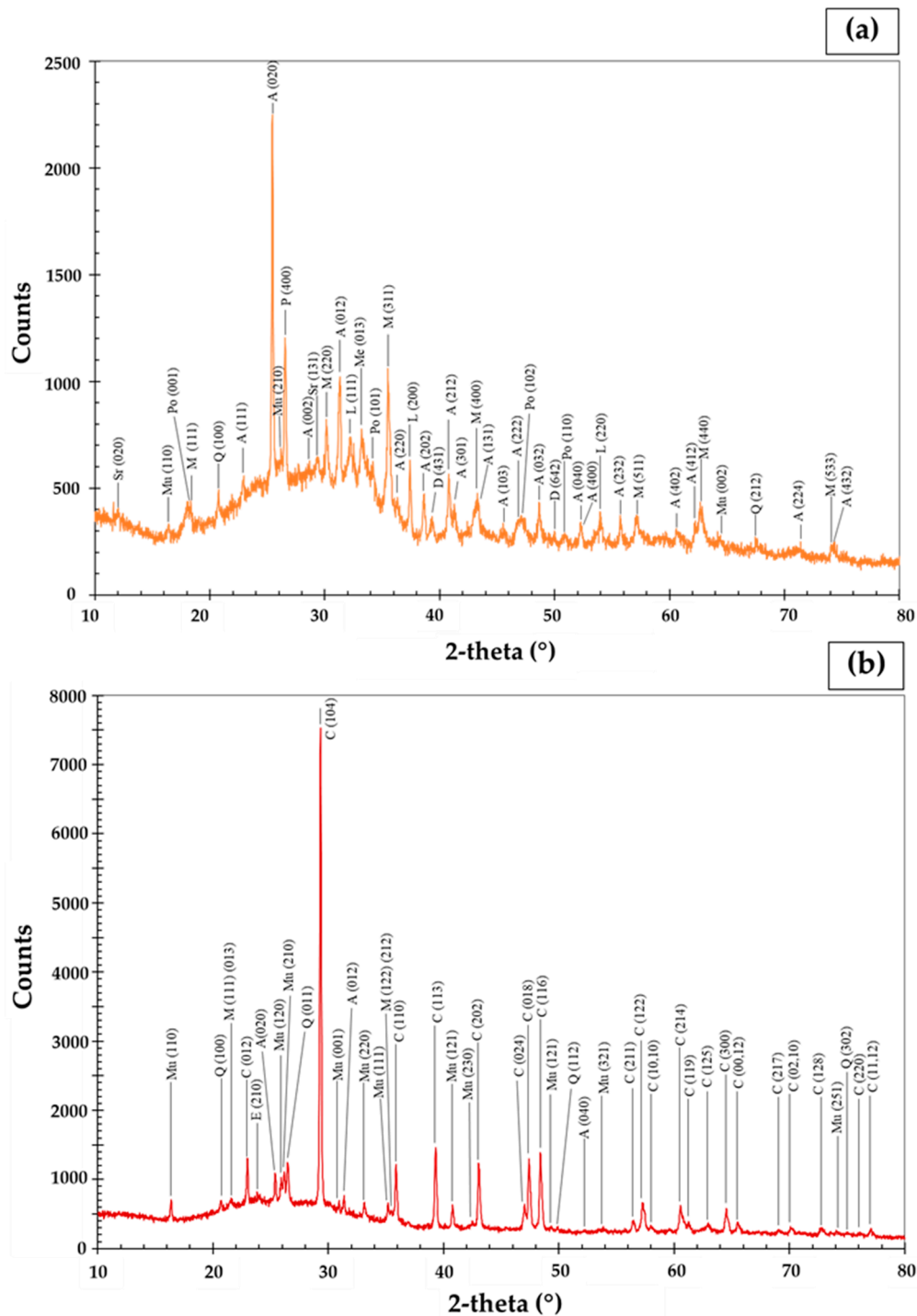


Figure 8. X-ray diffraction patterns of (a) fly ash sample and (b) bulk cenospheres showing mineral phases identified in the abbreviations: A—anhydrite, C—calcite, CS—calcium silicate, E—ettringite, L—lime, M—magnetite, Me—merwinite, Mu—mullite, P—potassium magnesium silicate, Po—portlandite, Q—quartz, Sr—srebrodolskite.

4. Conclusions

This work presented the investigation of the separation process and microstructure-chemical composition relationship of cenospheres separated from high calcium class C fly ash produced from Mae Moh power plant in Thailand. The result shows the percent cenospheres yield influenced by different preparation methods prior to sedimentation and settling separation. The effects of the fly ash-to-water ratio, stirring method, ultrasonication to deagglomerate the particles, and size sieving before the wet separation were studied. This work reported that the dependence of cenospheres recovery yield on the factor of fly ash/water ratio was more pronounced when incorporating low fly ash, from 1.25 wt.%–5 wt.%, in water medium. The maximum cenospheres recovery obtained was below the boundary of 3.5%. The results revealed no significant difference of the percent cenospheres recovery for those adopted methods. The comparison result clearly confirmed the limit of physical stirring-settling effect associated with the cenospheres content by nature that controlled the percent recovery. The majority of Mae Moh cenospheres, >80 wt.%, contained mostly the small particles of size <105 μm . The wall thickness of the cenospheres were found in the range of ~0.7 to 21.6 μm . The shell structures (single ring and porous) relating to the size and oxide composition were brought into a relationship. Different morphological features of cenospheres were described in terms of how the particles primarily formed in the furnace. The aggregates found on the cenosphere particles after the wet separation were identified and confirmed as a result of crystallization in the liquid medium. The pair dependence of $\text{SiO}_2\text{--Al}_2\text{O}_3$ contents and $\text{SiO}_2/\text{Al}_2\text{O}_3$ ratio– Al_2O_3 content was explained in the main correspondence with the varied particle size of cenospheres. The mineral phases and composition of the class C fly ash and the bulk cenospheres were characterized to commonly include both amorphous and crystalline phases.

Author Contributions: Conceptualization, S.Y.; methodology, S.Y.; formal analysis, S.Y.; investigation, S.Y. and P.T.; P.T. performed the experiment and material characterization; P.T. partially analyzed the material properties; data curation, S.Y.; S.Y. and P.T. participated in the data summary; writing—original draft preparation, S.Y.; writing—review and editing, S.Y.; visualization, S.Y.; supervision, S.Y.; project administration, S.Y.; funding acquisition, S.Y. All authors have read and agreed to the published version of the manuscript.

Funding: This research received funding by the Electricity Generating Authority of Thailand (EGAT), grant number 59-B104000-172-IO.SS03B3008261-MTEC and the National Metal and Materials Technology Center (MTEC), Project number P1651949 and P1751264. The APC was funded by MTEC, National Science and Technology Development Agency (NSTDA), Thailand.

Acknowledgments: This research was mainly supported by the Electricity Generating Authority of Thailand (EGAT), who kindly provided fly ash for this study. We also acknowledge MTEC, NSTDA, Thailand, for a partially funding support and the instrument facilities.

Conflicts of Interest: The authors declare no conflict of interest.

References

1. Jinawath, S.; Thitianan, C. Production of Multiphase Plaster and Anhydrite from Mae Moh Flue-Gas Desulphurised Gypsum. *Adv. Cem. Res.* **2002**, *14*, 121–126. [[CrossRef](#)]
2. Brigden, K.; Santillo, D.; Stringer, R. *Hazardous Emissions from Thai Coal-Fired Power Plants: Toxic and Potentially Toxic Elements in Fly Ashes Collected from Mae Moh Thai Petrochemical Industry Coal-Fired Power Plants in Thailand, 2002*; Greenpeace Research Laboratories, Department of Biological Sciences, University of Exeter: Exeter, UK, 2002.
3. Jayaranjan, M.L.D.; Hullebusch, E.D.V.; Annachhatre, A.P. Reuse Options for Coal Fired Power Plant Bottom Ash and Fly Ash. *Rev. Environ. Sci. Bio. Technol.* **2014**, *13*, 467–486. [[CrossRef](#)]
4. Punyawadee, V.; Ratana, P.; Winichakule, N.; Satienerakul, K. Costs and Benefits of Flue Gas Desulfurization for Pollution Control at the Mae Moh Power Plant, Thailand. *ASEAN Econ. Bull.* **2008**, *25*, 99–112. [[CrossRef](#)]
5. Tangtermsirikul, S. Development of fly ash usage in Thailand. *Soc. Soc. Manag. Syst. Int. J.* **2005**, *1*, 12.
6. Tangtermsirikul, S.; Kaewkhluab, T.; Jitvutikrai, P. A Compressive Strength Model for Roller-Compacted Concrete with Fly Ash. *Mag. Concr. Res.* **2004**, *56*, 35–44. [[CrossRef](#)]

7. Karasawa, A.; Suda, S.; Naito, H.; Fujiwara, H. Application of Fly Ash to Concrete Paving Block. In Proceedings of the 7th International Conference on Concrete Block Paving (PAVE AFRICA 2003), Sun City, South Africa, 12–15 October 2003.
8. Ohenoja, K.; Pesonen, J.; Yliniemi, J.; Illikainen, M. Utilization of Fly Ashes from Fluidized Bed Combustion: A Review. *Sustainability* **2020**, *12*, 2988. [[CrossRef](#)]
9. Sathonsaowaphak, A.; Chindaprasirt, P.; Pimraksa, K. Workability and Strength of Lignite Bottom Ash Geopolymer Mortar. *J. Hazard. Mater.* **2009**, *168*, 44–50. [[CrossRef](#)]
10. Antoni Klarens, K.; Indranata, M.; Jamali, L.A.; Hardjito, D. The Use of Bottom Ash for Replacing Fine Aggregate in concrete Paving Blocks. In Proceedings of the MATEC Web of Conferences, Hong Kong, China, 1–3 July 2017; p. 1005.
11. American Society for Testing and Materials. Standard Specification for Portland Cement. In *ASTM C150/C150M-20*; American Society for Testing and Materials: West Conshohocken, PA, USA, 2020.
12. EGAT Sustainability Report. Available online: <https://www.egat.co.th/en/images/sustainable-dev/csr-report/EGAT-CSR-Annual-2018-en/EGAT-CSR-2018.EN.pdf>. (accessed on 1 May 2020).
13. Vassilev, S.V.; Menendez, R.; Diaz-Somoano, M.; Martinez-Tarazona, M.R. Phase-Mineral and Chemical Composition of Coal Fly Ashes as a Basis for their Multicomponent Utilization. 2. Characterization of Ceramic Cenosphere and Salt Concentrates. *Fuel* **2004**, *83*, 585–603. [[CrossRef](#)]
14. Fomenko, E.V.; Anshits, N.N.; Solovyov, L.A.; Mikhaylova, O.A.; Anshits, A.G. Composition and Morphology of Fly Ash Cenospheres Produced from the Combustion of Kuznetsk Coal. *Energy Fuels* **2013**, *27*, 5440–5448. [[CrossRef](#)]
15. Li, Y.; Gao, X.; Wu, H. Ash Cenosphere from Solid Fuels Combustion. Part 2: Significant Role of Ash Cenosphere Fragmentation in Ash and Particulate Matter Formation. *Energy Fuels* **2013**, *27*, 822–829. [[CrossRef](#)]
16. Ngu, L.-N.; Wu, H.; Zhang, D.-K. Characterization of Ash Cenospheres in Fly Ash from Australian Power Stations. *Energy Fuels* **2007**, *21*, 3437–3445. [[CrossRef](#)]
17. Manocha, L.M.; Ram, K.A.; Manocha, S.M. Separation of Cenospheres from Fly Ashes by Flootation Method. *Eurasian Chemtech. J.* **2011**, *12*, 89–95. [[CrossRef](#)]
18. Ranjbar, N.; Kuenzel, C. Cenospheres: A Review. *Fuel* **2017**, *207*, 1–12. [[CrossRef](#)]
19. Blanco, F.; García, P.; Mateos, P.; Ayala, J. Characteristics and Properties of Lightweight Concrete Manufactured with Cenospheres. *Cem. Concr. Res.* **2000**, *30*, 1715–1722. [[CrossRef](#)]
20. Barbare, N.; Shukla, A.; Bose, A. Uptake and Loss of Water in a Cenosphere–Concrete Composite Material. *Cem. Concr. Res.* **2003**, *33*, 1681–1686. [[CrossRef](#)]
21. McBride, S.P.; Shukla, A.; Bose, A. Processing and Characterization of a Lightweight Concrete using Cenospheres. *J. Mater. Sci.* **2002**, *37*, 4217–4225. [[CrossRef](#)]
22. Liu, Z.; Zhao, K.; Tang, Y.; Hu, C. Preparation of a Cenosphere Curing Agent and Its Application to Foam Concrete. *Adv. Mater. Sci. Eng.* **2019**, *2019*, 1–9. [[CrossRef](#)]
23. Cardoso, R.; Shukla, A.; Bose, A. Effect of Particle Size and Surface Treatment on Constitutive Properties of Polyester-Cenosphere Composites. *J. Mater. Sci.* **2002**, *37*, 603–613. [[CrossRef](#)]
24. Chalivendra, V.B.; Shukla, A.; Bose, A.; Parameswari, V. Processing and Mechanical Characterization of Lightweight Polyurethane Composites. *J. Mater. Sci.* **2003**, *38*, 1631–1643. [[CrossRef](#)]
25. Wasekar, P.A.; Kadam, P.G.; Mhaske, S.T. Effect of Cenosphere Concentration on the Mechanical, Thermal, Rheological and Morphological Properties of Nylon 6. *J. Miner. Mater. Charact. Eng.* **2012**, *11*, 807–812. [[CrossRef](#)]
26. Ferdous, W.; Manalo, A.; Van Erp, G.; Aravinthan, T.; Ghabraie, K. Evaluation of an Innovative Composite Railway Sleeper for a Narrow-Gauge Track under Static Load. *J. Compos. Constr.* **2018**, *22*, 1–13. [[CrossRef](#)]
27. Tiwari, V.; Shukla, A.; Bose, A. Acoustic Properties of Cenosphere Reinforced Cement and Asphalt Concrete. *Appl. Acoust.* **2004**, *65*, 263–275. [[CrossRef](#)]
28. Yoriya, S.; Intana, T.; Tepsri, P. Separation of Cenospheres from Lignite Fly Ash Using Acetone-Water Mixture. *Appl. Sci.* **2019**, *9*, 3792. [[CrossRef](#)]
29. Danish, A.; Mosaberpanah, M.A. Formation Mechanism and Applications of Cenospheres: A Review. *J. Mater. Sci.* **2020**, *55*, 4539. [[CrossRef](#)]
30. Sahu, P.K.; Mahanwar, P.A.; Bambole, V.A. Effect of Hollow Glass Microspheres and Cenospheres on Insulation Properties of Coatings. *Pigment Resin Technol.* **2013**, *42*, 223–230. [[CrossRef](#)]

31. Joseph, K.V.; Francis, F.; Chacko, J.; Das, P.; Hebbar, G.S. Fly ash Cenosphere Waste Formation in Coal Fired Power Plants and Its Application as a Structural Material—A Review. *Int. J. Eng. Res. Technol.* **2013**, *2*, 1236–1260.
32. Shao, Y.; Jia, D.; Zhou, Y.; Liu, B. Novel Method for Fabrication of Silicon Nitride/Silicon Oxynitride Composite Ceramic Foams using Fly Ash Cenosphere as a Pore-Forming Agent. *J. Am. Ceram. Soc.* **2008**, *91*, 3781–3785. [[CrossRef](#)]
33. Gupta, N.W.E.; Mensah, P. Compression Properties of Syntactic Foams: Effect of Cenosphere Radius Ratio and Specimen Aspect Ratio. *Compos. Part A Appl. Sci. Manuf.* **2004**, *35*, 103–111. [[CrossRef](#)]
34. Li, Y.; Gao, X.; Wu, H. Further Investigation into the Formation Mechanism of Ash Cenospheres from an Australian Coal-Fired Power Station. *Energy Fuels* **2013**, *27*, 811–815. [[CrossRef](#)]
35. Hirajima, T.; Petrus, H.; Oosako, Y.; Nonaka, M.; Sasaki, K.; Ando, T. Recovery of Cenospheres from Coal Fly Ash using a Dry Separation Process: Separation Estimation and Potential Application. *Int. J. Miner. Process.* **2010**, *95*, 18–24. [[CrossRef](#)]
36. Petrus, H.; Hirajima, T.; Oosako, Y.; Nonaka, M.; Sasaki, K.; Ando, T. Performance of Dry-Separation Processes in the Recovery of Cenospheres from Fly Ash and their Implementation in a Recovery Unit. *Int. J. Miner. Process.* **2011**, *98*, 15–23. [[CrossRef](#)]
37. Sokol, E.; Maksimova, N.; Volkova, N.; Nigmatulina, E.; Frenkel, A. Hollow Silicate Microspheres from Fly Ashes of the Chelyabinsk Brown Coals (South Urals, Russia). *Fuel Process. Technol.* **2000**, *67*, 35–52. [[CrossRef](#)]
38. Ramme, B.W.; Noegel, J.J.; Rohatgi, P.K. Separation of Cenospheres from Fly Ash. U.S. Patent No. 8,074,804, 13 December 2011.
39. Kruger, R.; Toit, P. Recovery and Characterization of Cenospheres from South African Power Plants. In Proceedings of the Ninth International Ash Use Symposium, ACAA, Palo Alto, CA, USA, 3 January 1991; pp. 1–76.
40. Kolay, P.K.; Singh, D.N. Physical Chemical, Mineralogical, and Thermal Properties of Cenospheres from an Ash Lagoon. *Cem. Concr. Res.* **2001**, *31*, 539–542. [[CrossRef](#)]
41. Sarkar, A.; Rano, R.; Mishra, K.; Mazumder, A. Characterization of Cenospheres Collected from Ash-Pond of a Super Thermal Power Plant. *Energy Sources Part A Recover. Util. Environ. Eff.* **2007**, *30*, 271–283. [[CrossRef](#)]
42. Drozhzhin, V.S.; Shpirt, M.Y.; Danilin, L.D.; Kuvaev, M.D.; Pikulin, I.V.; Potemkin, G.A. Formation Processes and Main Properties of Hollow Aluminosilicate Microspheres in Fly Ash from Thermal Power Stations. *Solid Fuel Chem.* **2008**, *42*, 107–119. [[CrossRef](#)]
43. Fenelonov, V.B.; Mel'gunov, M.S.; Parmon, V.N. The Properties of Cenospheres and the Mechanism of their Formation during High-Temperature Coal Combustion at Thermal Power Plants. *Kona Powder Part. J.* **2010**, *28*, 189–208. [[CrossRef](#)]
44. Kolay, P.K.; Bhusal, S. Recovery of Hollow Spherical Particles with Two Different Densities from Coal Fly Ash and their Characterization. *Fuel* **2014**, *117*, 118–124. [[CrossRef](#)]
45. Żyrkowski, M.; Neto, R.C.; Santos, L.F.; Witkowski, K. Characterization of Fly-ash Cenospheres from Coal-Fired Power Plant Unit. *Fuel* **2016**, *174*, 49–53. [[CrossRef](#)]
46. American Society for Testing and Materials. Standard Specification for Coal Fly Ash and Raw or Calcined Natural Pozzolan for Use in Concrete. In *ASTM C618-12a*; American Society for Testing and Materials: West Conshohocken, PA, USA, 2012.
47. Bachus, R.C.; Terzariol, M.; Pasten, C.; Chong, S.H.; Dai, S.; Cha, M.S.; Kim, S.; Jang, J.; Papadopoulos, E.; Roshankhah, S.; et al. Characterization and Engineering Properties of Dry and Ponded Class-F Fly Ash. *J. Geotech. Geoenviron. Eng.* **2019**, *145*, 4019003. [[CrossRef](#)]
48. Ultracyc: True Volume and Density Analyzer Operating Manual. Available online: http://eodg.atm.ox.ac.uk/eodg/equipment/Pycnometer_user_manual.pdf (accessed on 22 July 2020).
49. Tepsri, P.; Chumphu, A.; Yoriya, S. High-Calcium Fly Ash Recovery from Wet-Stored Condition and its Properties. *Mater. Res. Express* **2018**, *5*, 115506. [[CrossRef](#)]
50. Fomenko, E.V.; Anshits, N.N.; Vasilieva, N.G.; Mikhaylova, O.A.; Rogovenko, E.S.; Zhizhaev, A.M.; Anshits, A.G. Characterization of Fly ash Cenospheres Produced from the Combustion of Ekibastuz Coal. *Energy Fuels* **2015**, *29*, 5390–5403. [[CrossRef](#)]
51. Anshits, N.; Mikhailova, O.; Salanov, A.; Anshits, A. Chemical Composition and Structure of the Shell of Fly Ash Non-Perforated Cenospheres Produced from the Combustion of the Kuznetsk Coal. *Fuel* **2010**, *89*, 1849–1862. [[CrossRef](#)]

52. Kutchko, B.G.; Kim, A.G. Fly Ash Characterization by SEM–EDS. *Fuel* **2006**, *85*, 2537–2544. [[CrossRef](#)]
53. Pintana, P.; Tippayawong, N.; Nuntaphun, A.; Thongchiew, P. Characterization of Slag from Combustion of Pulverized Lignite with High Calcium Content in Utility Boiler. *Energy Explor. Exploit.* **2014**, *32*, 471–482. [[CrossRef](#)]
54. Vassilev, S.V.; Vassileva, C.G. Mineralogy of Combustion Wastes from Coal-Fired Power Stations. *Fuel Process. Technol.* **1996**, *47*, 261–280. [[CrossRef](#)]
55. Hower, J.C.; Rathbone, R.F.; Robertson, J.D.; Peterson, G.; Trimble, A.S. Petrology, Mineralogy, and Chemistry of Magnetically-Separated Sized Fly Ash. *Fuel* **1999**, *78*, 197–203. [[CrossRef](#)]
56. Anshits, N.N.; Fedorchak, M.A.; Fomenko, E.V.; Mazurova, E.V.; Anshits, A.G. Composition, Structure, and Formation Routes of Blocklike Ferrospheres Separated from Coal and Lignite Fly Ashes. *Energy Fuels* **2020**, *34*, 3743–3754. [[CrossRef](#)]
57. McArthur, H.; Spalding, D. *Engineering Materials Science: Properties, Uses, Degradation, Remediation*, 1st ed.; Wookhead Publishing: Philadelphia, PA, USA, 2004.
58. Molar Mass, Molecular Weight and Elemental Composition Calculator. Available online: <https://www.webqc.org/mmolcalc.php> (accessed on 22 July 2020).
59. Vassilev, S.V.; Eskenazy, G.M.; Vassileva, C.G. Behaviour of Elements and Minerals during Preparation and Combustion of the Pernik Coal, Bulgaria. *Fuel Process. Technol.* **2001**, *72*, 103–129. [[CrossRef](#)]
60. Vassilev, S.V.; Eskenazy, G.M.; Vassileva, C.G. Contents, Modes of Occurrence and Behavior of Chlorine and Bromine in Combustion Wastes from Coal-Fired Power Stations. *Fuel* **2000**, *79*, 923–937. [[CrossRef](#)]
61. Zandi, M.; Russell, N.V. Design of a Leaching Test Framework for Coal Fly Ash Accounting for Environmental Conditions. *Environ. Monit. Assess.* **2007**, *131*, 509–526. [[CrossRef](#)]
62. Leelarungroj, K.; Likitlersuang, S.; Chompoorat, T.; Janjaroen, D. Leaching Mechanisms of Heavy Metals from Fly Ash Stabilised Soils. *Waste Manag. Res.* **2018**, *36*, 616–623. [[CrossRef](#)]
63. Hart, B.R.; Powell, M.A.; Fyfe, W.S.; Ratanasthien, B. Geochemistry and Mineralogy of Fly-Ash from the Mae Moh Lignite Deposit, Thailand. *Energy Sources* **2007**, *17*, 23–40. [[CrossRef](#)]
64. Egemen, E.; Yurteri, C. Regulatory Leaching Tests for Fly Ash: A Case Study. *Waste Manag. Res.* **1996**, *14*, 43–50. [[CrossRef](#)]
65. Baykal, G.; Saygili, A. A New Technique to Reduce the Radioactivity of Fly Ash Utilized in the Construction Industry. *Fuel* **2011**, *90*, 1612–1617. [[CrossRef](#)]
66. Nisnevich, M.; Sirotin, G.; Schlesinger, T.; Eshel, Y. Radiological Safety Aspects of Utilizing Coal Ashes for Production of Lightweight Concrete. *Fuel* **2008**, *87*, 1610–1616. [[CrossRef](#)]
67. Papaefthymiou, H.; Gouseti, O. Natural Radioactivity and Associated Radiation Hazards in Building Materials Used in Peloponnese, Greece. *Radiat. Meas.* **2008**, *43*, 1453–1457. [[CrossRef](#)]
68. Vassilev, S.; Menendez, R.; Alvarez, D.; Diaz-Somoano, M.; Martinez-Tarazona, M. Phase-Mineral and Chemical Composition of Coal Fly Ashes as a Basis for their Multicomponent Utilization. 1. Characterization of Feed Coals and Fly Ashes. *Fuel* **2003**, *82*, 1793–1811. [[CrossRef](#)]
69. Li, Y.; Wu, H. Ash Cnosphere from Solid Fuels Combustion. Part 1: An Investigation into its Formation Mechanism using Pyrite as a Model Fuel. *Energy Fuels* **2012**, *26*, 130–137. [[CrossRef](#)]
70. Gupta, S.; Gupta, R.; Bryant, G.; Wall, T. The Effect of Potassium on the Fusibility of Coal Ashes with High Silica and Alumina Levels. *Fuel* **1998**, *77*, 1195–1201. [[CrossRef](#)]
71. Vassilev, S.V.; Vassileva, C.G.; Karayigit, A.I.; Bulut, Y.; Alastuey, A.; Querol, X. Phase-Mineral and Chemical Composition of Fractions Separated from Composite Fly Ashes at the Soma Power Station, Turkey. *Int. J. Coal Geol.* **2005**, *61*, 65–85. [[CrossRef](#)]
72. Fischer, R.X.; Schneider, H.; Schmucker, M. Crystal Structure of Al-Rich Mullite. *Am. Miner.* **1994**, *79*, 983–990.

